Atmos. Chem. Phys. Discuss., 13, 9615–9652, 2013
www.atmos-chem-phys-discuss.net/13/9615/2013/
doi:10.5194/acpd-13-9615-2013

Atmospheric Chemistry and Physics
Open Access
Discussions

This discussion paper is/has been under review for the journal Atmospheric Chemistry and Physics (ACP). Please refer to the corresponding final paper in ACP if available.

Mid-latitude cirrus classification at Rome Tor Vergata through a multi-channel Raman–Mie–Rayleigh lidar

D. Dionisi[1,2], P. Keckhut[1], G. L. Liberti[2], F. Cardillo[2], and F. Congeduti[2]

[1]Laboratoire Atmosphères, Milieux, Observations Spatiales-IPSL, UMR8190, CNRS/INSU, UVSQ-UPMC, UniverSud Paris, Guyancourt, France
[2]Istituto di Scienze dell'Atmosfera e del Clima, Consiglio Nazionale delle Ricerche, Roma, Italy

Received: 6 March 2013 – Accepted: 4 April 2013 – Published: 11 April 2013

Correspondence to: D. Dionisi (davide.dionisi@latmos.ipsl.fr)

Published by Copernicus Publications on behalf of the European Geosciences Union.

Abstract

A methodology to identify and characterize cirrus clouds has been developed and applied to the multichannel-multiwavelength Rayleigh–Mie–Raman (RMR) lidar in Rome-Tor Vergata (RTV). A set of 167 cirrus cases, defined on the basis of quasi-stationary temporal period conditions, has been selected in a dataset consisting of about 500 h of nighttime lidar sessions acquired between February 2007 and April 2010. The derived lidar parameters (effective height, geometrical and optical thickness and mean back-scattering ratio) and the cirrus mid-height temperature (estimated from the radiosoundings of Pratica di Mare, WMO site #16245) of this sample have been analyzed by the means of a clustering multivariate analysis. This approach identified four cirrus classes above the RTV site: two thin cirrus clusters in mid and upper troposphere and two thick cirrus clusters in mid-upper troposphere. These results, which are very similar to those derived through the same approach in the lidar site of the Observatoire of Haute Provence (OHP), allows characterizing cirrus clouds over RTV site and attests the robustness of such classification.

To have some indications about the cirrus generation methods for the different classes, the analyses of the extinction-to-backscatter ratio (lidar ratio, LR_{eff}), in terms of the frequency distribution functions and depending on the mid-height cirrus temperature have been performed. This study suggests that smaller (larger) ice crystals compose thin (thick) cirrus classes. This information, together with the value of relative humidity over ice (110 ± 30 %), calculated through the simultaneous WV Raman measurements for the mid-tropospheric thin class, indicates that this class could be formed by an heterogeneous nucleation mechanism.

The RTV cirrus results, re-computed through the cirrus classification by Sassen and Cho (1992), shows good agreement to other mid-latitude lidar cirrus observation for the relative occurrence of subvisible (SVC), thin and opaque cirrus classes (10 %, 49 % and 41 %, respectively). The overall mean value of cirrus optical depth is 0.37 ± 0.18 , while

ACPD
13, 9615–9652, 2013

most retrieved LR_{eff} values ranges between 10–60 sr and the estimated mean value is 31 ± 15 sr, similar to LR values of lower latitude cirrus measurements.

The obtained results are consistent with previous studies conducted with different systems and confirm that cirrus classification based on a statistical approach seems to be a good tool both to validate the height-resolved cirrus fields, calculated by models, and to investigate the key processes governing cirrus formation and evolution. These are fundamental elements to improve the characterization of the cirrus optical properties and, thus, the determination of their radiative impact.

1 Introduction

Despite extensive researches have been dedicated to the cirrus observation in conjunction with relevant parameters (temperature, humidity, aerosols, wind, waves, etc.) in the last decades, the report of the International Panel for Climate Change (IPCC, Solomon et al., 2007) demonstrated that the estimation of cirrus radiative impact is still one of the most largest source of uncertainty in global climate models (GCMs) parameterizations. Furthermore, it is not well known the exact role of the different parameters in the formation of cirrus clouds (Lohmann et al., 2004). To understand the effects of this type of clouds on the Earth's climate, it is necessary to observe and characterize their properties. In particular, cirrus vertical distributions determine their local cooling or warming effects (Khvorostyanov and Sassen, 2002). Climate models are sensitive to even small changes in the cirrus coverage and the numerical representation of cirrus in GCMs were not accurately constrained by available satellite data (Zhang et al., 2005), before the recently use of space-borne lidar measurements (Chepfer et al., 2008). Furthermore in-situ observations constitute a demanding and expensive operation and cannot provide a representative database to derive consistent cirrus climatology. In summary, in GCM cloud prognostic schemes, there are still open questions regarding cirrus. These issues are related to both, a lack of reliable observations and to the shortcomings of the forecast models to simulate ice clouds (Immler et al., 2008).

ACPD
13, 9615–9652, 2013

Lidar technique can detect cirrus with high spatial and temporal resolution, providing accurate information on their vertical distribution and, therefore, it could be used to develop highly resolved cirrus databases. In particular, lidar measurements give access to cirrus boundaries, vertical thickness (with resolution of 10 to 100 m), optical depth and cirrus backscattering ratio, which is related to the number of particles, their size distribution, shape, particle habit and phase.

In the last two decades the observation and characterization of cirrus clouds through the lidar technique have been largely performed in several regions of the globe both in terms of campaigns and of regular observations (Sassen and Campbell, 2001; Goldfarb et al. 2001; Wang and Sassen, 2002; Immler et al., 2002; Seifert et al., 2007).

Since 2006, cirrus clouds are continuously and globally monitored through Cloud-Aerosol Lidar with Orthogonal Polarization (CALIOP) installed on Cloud-Aerosol Lidar and Infrared Pathfinder Satellite Observations (CALIPSO) satellite. These observations are largely exploited in tropical regions (Haladay et al., 2009; Sassen et al., 2009; Riihimaki et al., 2010), where cloud vertical distribution is not well known. At mid-latitude, lidar cirrus information seems to be consistent from ground and space (Dupont et al., 2010). Although the frequency of occurrence of cirrus clouds is lower at mid-latitudes than in the tropics, it is important to characterize accurately their vertical distribution and understand associated processes of formation and evolution in order to properly take them into account in climate numerical models.

Based on the optical depth (τ), the (COX?) classification scheme of Sassen and Cho (1992) divides cirrus in subvisible (SVC), thin and opaque ($\tau < 0.03$, $0.03 < \tau < 0.3$ and $\tau > 0.3$, respectively). A lidar climatogy of mid-latitude cirrus in Utah has been derived by Sassen and Campbell (2001). In this work, detected cirrus were related to three different weather patterns: zonal jet stream flow, strong amplitude ridge and cases of split-jet flow. However, the link between these patterns and the processes of cirrus formation is difficult to deduce.

Recent researches performed through the lidar at Observatory of Haute Provence (OHP) have been aimed to use lidar database to characterize mid-latitude cirrus. In particular, statistical description of cirrus cloud at Mid-latitude was derived (Goldfarb et al., 2001) and three distinct cirrus classes with different optical properties were identified (Keckhut et al., 2006).

This type of classification could be useful both for the validation of height-resolved cirrus fields as reproduced by models and for the investigation of the key processes controlling cirrus formation and evolution. In fact any parameterization of cirrus cloud should take into account the generating mechanism of cirrus to well characterize cirrus optical properties (Whiteman et al., 2004) and their radiative impact. The French analyses suggested that cirrus morphologies can be linked to the mechanisms of their formation.

The study conducted with the lidar system located at Rome-Tor Vergata (RTV) fits in with this contest. In fact, the aim has been to utilize the lidar database acquired independently for other purposes (i.e. Raman water vapor measurements in troposphere and Rayleigh/Raman temperature measurements in upper atmosphere), to derive information on cirrus clouds. In fact, although the multi-channel configuration of the Rayleigh–Mie–Raman (RMR) lidar is well suited to characterize cirrus clouds, this system, before this work, was never been addressed to this type of studies. Furthermore a detailed study on cirrus clouds have not been conducted yet above this region (i.e. central Italy), except for the work of Gobbi et al. (2004), which provided a first statistics of cirrus occurrence during one year of lidar data over RTV sites without discriminating the types of the observed cirrus.

Given these considerations, the objective of this study has been to adapt and apply a methodology to identify and characterize cirrus, using measurements of RMR lidar system. The statistical procedure adopted is based on a clustering multivariate analysis previously developed to the lidar cirrus observation at OHP (Keckhut et al., 2006). This approach has been applied to approximately 500 h of nighttime lidar sessions acquired between February 2007 and April 2010 by the RMR lidar system.

The obtained results and their comparison to those derived by the OHP lidar permitted both to characterize the cirrus over RTV site and to verify the robustness of OHP climatology while only 600 km separate both sites.

With the objective of analyzing the optical properties of the identified classes, a sub-sample of the cirrus observation has, then, been studied in terms of the lidar ratio (i.e. the extinction-to-backscatter ratio). Finally, the RTV cirrus results have been computed through the Sassen and Cho classification and compared to other mid-latitude lidar cirrus dataset.

The paper is organized as follows: Sect. 2 consists in a brief summary of the characteristics of the RMR channels used for this study and in a detailed description of the cirrus retrieval algorithms developed and applied to RTV lidar data. Section 3 addresses the multivariate clustering method and the results obtained. In particular cirrus classification at RTV is presented, compared to the OHP and a sub-sample of cirrus classes are characterized and discussed in terms of their lidar parameters. Finally, in Sect. 4, the results and the perspectives of this approach are resumed.

2 Instrument and cirrus retrieval algorithm description

2.1 The Rayleigh–Mie–Raman lidar system

The RMR lidar located in the suburban area of Rome (41.8° N, 12.6° E, and 107 m altitude), in the Institute of Atmospheric Sciences and Climate (ISAC), utilizes a Nd:YAG laser with second and third harmonics generators which emits two pulsed beams in the green (532.2 nm, 200 mJ energy per pulse) and in the UV (354.8 nm, 400 mJ energy per pulse), with 10 Hz repetition rate and $\sim$7 ns pulse width. The green beam is used to receive the elastic backscatter from the air molecules and aerosol particles; the UV beam is used to obtain Raman backscattering signals from water vapor (WV) and nitrogen molecules and to calculate WV mixing ratio. A multiple telescope configuration, shown in Fig. 1, is adopted in the receiver to collect the signal return from

ACPD
13, 9615–9652, 2013

different altitude layers. A detailed description of the system is reported in Congeduti et al. (1999) and in Dionisi et al. (2010), and only the characteristics of channels used in this work are described here. A 15 cm aperture telescope, addressed to sense troposphere (0.5–14 km), has been used to collect 532 nm elastic backscattered signal, whereas the 387 nm nitrogen Raman signal has been acquired through the employment of a 30 cm telescope (lower channel) and an array of nine 50 cm telescopes (upper channel). Data merging between these two channels has been obtained as follows: due to the effect of the chopper installed in the upper channel, below 7 km data from the lower channel are selected; between 7 and 9 km data are selected considering the channel with the largest SNR; above 9 km only data acquired by the upper channel is considered. The acquisition vertical and temporal resolutions are, respectively, 75 m and 1 min. The characteristics of the system are resumed in Table 1.

2.2 Cirrus principal parameters

The procedure developed allows characterizing cirrus through 5 lidar principal parameters: height of cirrus boundaries (z_{top} and z_{bottom}), the geometrical ($\mathrm{d}z = z_{\mathrm{top}} - z_{\mathrm{bottom}}$) and optical ($\mathrm{d}\tau$) depth and the backscattering ratio profile (SR). The last term is defined by the expression:

$$\mathrm{SR}(\lambda, z) = \frac{\beta_{\mathrm{aer}}(\lambda, z) + \beta_{\mathrm{mol}}(\lambda, z)}{\beta_{\mathrm{mol}}(\lambda, z)}, \tag{1}$$

where β_{aer} and β_{mol} are the backscattering coefficients due to aerosol and molecules.

Using the ratio of the elastic $\mathrm{S}(\lambda_0)$ and Raman nitrogen $\mathrm{S}(\lambda_\mathrm{N})$ backscattered lidar signals at two different heights (z andz_0 with $z > z_0$) and assuming that $\beta_{\mathrm{aer}} \ll \beta_{\mathrm{mol}}$ at z_0 (clear air condition), it has been demonstrated (Ansmann et al., 1992) that:

$$\frac{\mathrm{S}(\lambda_0, z) \cdot \mathrm{S}(\lambda_\mathrm{N}, z_0)}{\mathrm{S}(\lambda_\mathrm{N}, z) \cdot \mathrm{S}(\lambda_0, z_0)} \cdot \frac{1}{\tau_{\mathrm{diff}}^{\mathrm{mol}}[z_0 : z]} = \frac{\beta_{\mathrm{aer}}(\lambda_0, z) + \beta_{\mathrm{mol}}(\lambda_0, z)}{\beta_{\mathrm{mol}}(\lambda_0, z)} \cdot \tau_{\mathrm{diff}}^{\mathrm{mol}}[z_0 : z] \approx \mathrm{SR}(z). \tag{2}$$

ACPD
13, 9615–9652, 2013

In our case, $\tau_{\text{diff}}^{\text{mol}}[z_0 : z]$, which describes the molecular differential transmission between the laser emitted (λ_0) and the received Raman nitrogen (λ_R) wavelength at z_0 and at z, is determined from radiosonde data. Since the aerosol differential transmission term, $\tau_{\text{diff}}^{\text{aer}}[z_0 : z]$, can be approximated to be equal to 1 outside (in case of negligible aerosol background) and inside (ice particle scattering, Van de Hulst, 1957) the cirrus, the first term in Eq. (2) is equal to SR.

Cirrus boundaries are identified applying the so-called Discrete Wavelet Transform (DWT), using a zero-order wavelet (Haar function). This function, usually adopted for planet boundary layer (PBL) studies (Brooks, 2003; Haij et al., 2007), is defined by:

$$h\left(\frac{z-b}{a}\right) = \begin{cases} 1 : b - \frac{a}{2} \leq z \leq b \\ -1 : b \leq z \leq b + \frac{a}{2} \\ 0 : \text{elsewhere} \end{cases} \tag{3}$$

where a and b are, respectively, the width and the dilation (the point where the function is centered) of the wavelet. The coefficients $W_B(a,b)$, which are the results of the convolution between SR and h, are:

$$W_B(a,b,z) = a^{-1} \int_{Z-a/2}^{z+a/2} \text{SR}(\lambda, z') \cdot h\left(\frac{z'-b}{a}\right) \text{d}Z'. \tag{4}$$

If SR is in phase (anti-phase) with the Haar wavelet, the convolution product shows a maximum (minimum), and these points can be used to determine the inflection points of the SR, which, in turns, correspond to the bottom (top) of the cirrus.

Figure 2 shows the application of this technique to the case of cirrus observed during the night of 5 July 2012. In the right panel, the SR profile, integrated for 42 min, is reported, while the corresponding $W_B(a,b,z)$ is depicted on the left panel. The dashed horizontal lines indicate the inflection points corresponding to the cirrus boundaries.

Due to the scale of the structures observed (at least some hundreds of meters), the value of 375 m (5 lidar points) has been fixed for the width of the wavelet, having verified that the variation of this parameter (from 225 to 975 m) does not significantly affect the identification of boundaries.

The presence of a cirrus is revealed when the absolute values of $W_B(a,b,z)$ exceed a fixed threshold (W_s) and the temperature is below $-25\,^{\circ}$C. The value of W_s has been chosen through a study of sensibility that considered the signal to noise ratio (SNR) of SR profile. The employment DWT technique, being based on an integral quantity instead of a derivative, it is much less prone to noise-induced detections than a numerical differentiation technique based on the direct analysis of SR, which, in upper troposphere and in case of strong extinguishing cirrus, is often subjected to low values of SNR.

The effective height (z_{cir}) is defined as (Chen at al., 2002):

$$z_{\mathrm{cir}} = \frac{\int_{z_{\mathrm{base}}}^{z_{\mathrm{top}}} z' \cdot \mathrm{SR}(z')\mathrm{d}z'}{\int_{z_{\mathrm{base}}}^{z_{\mathrm{top}}} \mathrm{SR}(z')\mathrm{d}z'}, \tag{5}$$

namely the SR mass center of the cirrus.

Optical depth (τ) has been estimated using the SR profile inside the cirrus with a fixed a-priori value of lidar ratio (LR, Goldfarb et al., 2001):

$$\tau_{\mathrm{cir}} = \mathrm{LR} \cdot \frac{\mathrm{d}\sigma_{\mathrm{Ray}}}{\mathrm{d}\Omega} \int_{z_{\mathrm{base}}}^{z_{\mathrm{top}}} n_{\mathrm{air}}(z) \cdot (\mathrm{SR}(z) - 1)\,\mathrm{d}z, \tag{6}$$

where $\mathrm{d}\sigma_{\mathrm{Ray}}/\mathrm{d}\Omega = 5.7 \times 10^{-32}\,\mathrm{m}^2\,\mathrm{sr}^{-1}$ is the backscattering differential molecular cross section, n_{air} is the molecular density derived by radiosounding measurements and LR

ACPD
13, 9615–9652, 2013

= 18.2 sr (Platt and Diley, 1984). The value of LR will be discussed in Sect. 3.2. If one of the advantages of this particle integration (PI) method is a low sensibility to SNR (Cadet et al., 2005), on the other hand, it should be stressed that LR strictly depends on the ice crystal optical properties and the employment of an a-priori value of LR (i.e. assumption of fixed physical properties) could introduce some errors on the derived values. Furthermore, due to the vertical pointing of the RMR laser, also the specular reflection effect could affect the value of τ_{LR}.

The evaluation of τ has been performed also using the extinction of Raman signal below and above the cirrus (Raman method, Ansmann et al., 1992):

$$\tau_{Rm} = -\frac{1}{2\eta} \cdot \ln\left(\frac{S_{N\_cal}[z_{top} : Z_2]}{S_{N\_cal}[z_1 : z_{base}]}\right), \tag{7}$$

where S_{N_cal} is the Raman nitrogen signal calibrated with the radiosonde profile in the atmospheric layers below ($z_1 : z_{base}$) and above ($z_{top} : z_2$) the cirrus (where $z_{base} - z_1$ and $z_2 - z_{top}$ are equal to 500 and 800 m, respectively), corrected from the molecular extinction and assuming negligible aerosol background, and η is the corrective factor that takes into account the multiple scattering (MS) effect. Using only a single lidar signal, the Raman method could be significantly influenced by MS (Wandinger, 1998). This effect depends on several factors (laser divergence, field of view of the receiver, laser penetration depth, cloud height, particle size distribution, and crystal shapes). Following Seifert et al. (2007), a MS factor $\eta = 0.60 \pm 0.1$ for cirrus geometrical depths < 1 km and $\eta = 0.7 \pm 0.1$ for larger geometrical depths has been adopted in this analysis. The applicability of the Raman method is limited by the uncertainty due to the weak Raman signal intensity (three order of magnitude less than elastic backscattered signal).

To reduce the statistical error and obtain reasonable SNR values in the upper troposphere, a temporal integration is performed on lidar signal before the estimation of the cirrus parameters listed above. The approach adopted consists in analyzing the time series of the optical depth (estimated with PI method) of the mid and upper troposphere

ACPD
13, 9615–9652, 2013

(between 7 and 12/13 km, approximately) with a temporal resolution of the original raw data to research discontinuity points in order to define Quasi-Stationary Temporal Periods (QSTP) regarding statistical variability (Lanzante, 1996). As proposed by Hoareau et al. (2009), data analyses are then performed on these integrated periods to derive accurate optical cirrus properties. To obtain consistent results, this approach should be applied to a statistically meaningful number of points, thus only temporal periods greater than 15 min (15 points) are considered. The employment of this analysis has also permitted to homogenize lidar datasets, applying clustering analysis to the same sample in terms of statistical variability. In this work, 93 nighttime lidar sessions acquired between February 2007 and April 2010 have been analyzed through this procedure and 167 QSTP have been identified.

High-resolution radiosounding data (Vaisala RS92) were used from the Italian Meteorological Service in Pratica di Mare (25 km south – west of Tor Vergata) to add complementary description of the background conditions (e.g. density, mid-cirrus height temperature) to the lidar results. The height of the tropopause has been estimated using the definition of thermal tropopause (WMO, 1957).

2.3 Multivariate clustering analysis

Once retrieved principal parameters of cirrus quasi-stationary periods, different statistical methods could be used to identify cirrus classes. An analysis in terms of probability distribution function (PDF), which revealed non-Gaussian multimode distributions, has been firstly made. However, as showed by Keckhut et al. (2006), this analysis is not adequate to determine objectively cirrus classes, because cross correlation between each parameter has to be taken into account. On the contrary multivariate analysis (MA) is a good candidate to discriminate the presence of cirrus classes. Thus, following the methodology applied to OHP cirrus dataset (Keckhut et al., 2006) and, recently, to sub-tropical cirrus clouds from Reunion Island lidar dataset (Hoareau et al., 2012), the successive use of principal component analysis (PCA), hierarchical clustering method (HCM) and discriminant factor analysis (DFA) has been employed to analyze the cirrus

Discussion Paper | Discussion Paper | Discussion Paper | Discussion Paper |

ACPD
13, 9615–9652, 2013

Mid-latitude cirrus classification at Rome Tor Vergata

D. Dionisi et al.

observations sampled by TVR lidar and radiosoundings. A detailed description of the methodology is reported in Borchi and Marenco (2001), while here only the main characteristics of the adopted procedure are reported.

The PCA is used to reduce data by finding the linear combinations of the original variables accounting as much as possible of the total variance of the original data (Jolliffe, 1986). Through this analysis new uncorrelated variables (principal components) are defined and used, as parameters describing the observations, in HCM. The aim of HCM is to group observations into clusters, aggregating them hierarchically. This method uses Euclidean distance as dissimilarity measure between observations and the Ward's method (Ward, 1963) for the agglomerative clustering method. To ensure the robustness of these results, a discriminant factor analysis (DFA), which identifies the optimal set of orthogonal projection axes that best discriminate the classes, is performed.

3 Results

3.1 Cirrus classification

Cirrus clouds have been detected in 47 % of the 93 analyzed lidar session (daily occurrence, which is the number of cirrus detections divided by the total number of measurements), whereas the absolute occurrence is 30 % (i.e. the ratio of cirrus detection time on the total lidar measurement time). Before entering into statistical details, it is important to specify that nighttime lidar measurements were performed only in absence of precipitation and of lower tropospheric (below 4 km) thick extinguishing clouds. However Dupont et al. (2010) have shown with CALIOP (Cloud-Aerosol Lidar with Orthogonal Polarization) data that neither nighttime nor ground conditions introduced any obvious bias in cirrus climatology using ground-based lidar at mid-latitudes. It is also noteworthy that for 17 % of cirrus cases, multi-layer cirrus have been observed and analyzed separately when more than 500 m of clear air appeared between them. Table 2 summarizes the dataset analyzed through the multivariate clustering.

The cirrus parameters of the 167 QSTP, processed by the MA approach, are: mid-cirrus height, geometrical depth, mid-cirrus height temperature, SR mean intensity, relative height (the difference between cirrus top height and thermal tropopause). These parameters have been chosen following Keckhut et al. (2006). In particular, since the required assumptions on the estimation of the cirrus τ (e.g. effects of multiple scattering, weakness of the signal in case of the Raman method and a-priori and fixed value of LR in case of PI method) produce a larger uncertainty compared to the other parameters, this variable has not been considered at this stage. However, it has been verified that the use of τ as one of the five parameters led to the same results in terms of cirrus classes, most probably because τ is not independent from the measured parameters as geometrical depth and SR.

The three first principal components (PCs) identified by PCA take into account almost the 98 % of the cumulative variance, in particular PC1 and PC2 representing 89 % (52 and 37 %, respectively). The results obtained by MA are resumed in Fig. 3, where the observations are projected on two orthogonal discriminating axes F1 and F2, obtained by the DFA. Different colors highlight the presence of several clusters, identified by HCM and confirmed by DFA. These clusters correspond to five different cirrus classes, whose main characteristics are reported in Table 3, where the mean and standard deviation for all parameters are listed.

The classes I and III, which refer to thin cirrus observed in mid and upper troposphere, respectively, are characterized by low values of SR mean intensity, geometrical and optical depth. In contrast, IIa and IIb represent thick cirrus, sensed between 9 and 10 km, with larger vertical extension and higher values of SR and optical depth.

Another characteristic that distinguishes thick from thin cirrus classes is the frequency of occurrence, which is lower for thin cirrus both if they are observed in medium and in high troposphere. The very rare occurrence of the last class (IV), characterized by very high values of the mean backscattering term that could be caused by specular

ACPD
13, 9615–9652, 2013

reflection effects, cannot permit to assess if this class can be considered as a distinct class and it will not be further discussed in this work.

The last part of Table 2 reports the results of the same analysis performed using OHP dataset for more than ten years of lidar measurements (Hoareau et al., 2013). The comparison between the French and Italian cirrus classification points out the high similarities for the two classes of thin cirrus identified on both sites (class I and class III, respectively). In fact, for the two classes, the values of mean height and geometrical thickness are in very good agreement.

In contrast with OHP results, the RTV classification seems to split thick cirrus cloud OHP class (II) at 9.8 km, in two distinct classes (IIa anb IIb) located at 8.8 and 10.2 km. However, combining the values of mean height and geometrical thickness of these two classes, weighted by the occurrence, it is possible to obtain a class with the values of mean height and thickness (9.6 and 3.4 km, respectively) that is closer to the class II observed at OHP.

The absolute occurrence of the classes between the two sites are also different: at RTV site, thick cirrus (class IIa and IIb) occurs 15 % of the times (11 % at the OHP), thin tropopause cirrus (class III) are observed only 9 % (15 % at OHP) and also middle tropospheric thin cirrus (class I) are less present over the RTV (5 % vs 10 %).

3.2 Cirrus optical properties and attribution

The optical properties of each cirrus class have been studied through the combined use of elastic and Raman nitrogen lidar channels. In particular, to have an homogenous dataset, the values of the effective LR (LR_{eff}, the ratio between the extinction and the integrated value of SR inside the cirrus) have been estimated only for cirrus cases with $\Delta\tau_{Rm}/\tau_{Rm} \leq 30\,\%$, where $\Delta\tau_{Rm}$, the error associated to τ_{Rm}, is calculated applying the propagation error formula to the Eq. (7) (considering the signal random errors). Only 107 cirrus cases (65 % of the total) have been considered. The number of cirrus cases analyzed, the values of the mean for τ_{LR}, τ_{Rm}, LR_{eff} and the relative position of

Discussion Paper | Discussion Paper | Discussion Paper | Discussion Paper |
ACPD
13, 9615–9652, 2013
Mid-latitude cirrus classification at Rome Tor Vergata
D. Dionisi et al.

SR mass center compared to the mean geometric height are listed for each class in Table 4.

For the subsample, the τ_{LR} mean values for each classes are higher than those computed for the entire sample. This is consistent, because small values of optical depth are, generally, more affected by the statistical error and, thus, discarded. The estimated τ_{Rm} is higher in comparison to τ_{LR} for all the classes. This result seems to indicate that the used LR_{ap} is not adequate to describe the mean cirrus optical properties and a higher value should be employed. In particular, the values of LR_{eff} for thick and thin cirrus classes are very similar (31–32 and 28–29 sr, respectively). However, as shown by the Figs. 5 and 6 that will be discussed afterwards, it is worth noting that the errors associated to LR_{eff} values are characterized by a large variability that should be taken into account. With this aim it has been assumed that each value has a Gaussian shape, which is determined by LR_{eff} and the associated error ΔLR_{eff} where in the Gaussian function are equal to the expected value μ and the square root of the variance σ^2, respectively. The Fig. 4 depicts the frequency distribution functions of LR_{eff} calculated for the four classes.

Classes IIa, IIb and III have the distribution centered between 20 and 40 sr (68 %, 72 % and 55 % of the LR_{eff} are included in this range, respectively), with the latter differing from the two former classes for a less peaked shape and almost 30 % of the values included between 0 and 20 sr. These two characteristics are stressed in the class I where, in addition to a more flattened shape, the LR_{eff} values are almost equally distributed between two ranges 0–20 and 20–40 sr (43 % and 37 %, respectively).

The similar results for classes IIa ad IIb confirm the possible existence of only one bigger class of thick cirrus, while the flattened shape of classes I and III highlights that the estimated effective lidar ratio is characterized by larger errors (smaller values of τ_{Rm}, and then of LR_{eff}, are more affected to the signal fluctuations due to the statistical error noise than larger values of τ_{Rm}). However, it is interesting to highlight the higher probability to find the LR_{eff} in the range 0–20 sr, for these thin cirrus classes. In fact, according to model simulations (Reichardt et al., 2002), crystals with high values of

ACPD
13, 9615–9652, 2013

lidar ratio are bigger and exhibit higher degree of irregularity than crystals with low values. Following this hypothesis and from the analysis of the LR_{eff} distribution, one may conclude that classes III and I could be composed by crystals smaller and more regular in shape respect to the crystals composing the classes IIa and IIb.

Different methods of cirrus generations, which reflect in different LRs (Whiteman et al., 2004), could have caused these differences. If several case studies (Keckhut et al., 2005; Montoux et al., 2010) relate the formation of the III class to large-scale transport processes of moist tropical upper tropospheric air masses, the origin of class I has not been studied yet. The differences of LR_{eff} distributions and of the relative positions of SR mass for the classes I and III (0.50 and 0.56, in Table 4) seems to suggest a different processes of ice crystal generation and distribution inside these clouds.

Figure 5 presents the LR_{eff} values as a function of mid-cloud temperature (T_{mc}) for class I (first row) and class III (second row) in terms of a scatter plot (first column, where the LR_{eff} with the associated uncertainties are plotted in function of T_{mc}) and of frequency distribution representation (second column, where the LR_{eff} values, weighted with their uncertainties, are depicted with respect to midcloud temperature intervals of 5 K). The tropopause thin cirrus class is characterized by a small temperature interval (only 10 K) and a not significative dependence between LR_{eff} and T_{mc}. On the contrary, although the amplitude of the error bars is not negligible, the mid-tropospheric thin cirrus class exhibits a larger temperature interval (20 K) and trend of LR_{eff} increasing from approximately 10 to 45 sr with temperature decreasing between −25 and −40 °C.

Whiteman et al. (2004) measured a similar dependence in this temperature range for non-hurricane cirrus cases, whose origins were attributed to local sources.

One of the main applications of the RMR lidar is to provide atmospheric WV measurements in the whole troposphere (Congeduti et al., 1999) and, recently, a semi-automatic parametric calibration procedure (Dionisi et al., 2010) allowed calibrating the entire dataset (2003–2011). Thus, deriving the WV mixing ratio from the Raman signals acquired together with the cirrus elastic channel and the temperatures from Pratica di

Mare radiosoundings, it has been possible to estimate the mean relative humidity over ice (RHi) for the class I. The retrieved value (RHi = 110 ± 30 %) is consistent with those estimated by Immler et al. (2007) inside subvisible (SVC) and contrails clouds at Lindenberg/Germany and, in general, to those measured in Northern Hemisphere (NH) during INCA experiment (Strom et al., 2003). It has to be noted that this value was obtained assuming that, although the sites are not collocated, the temperature measured by the radiosonde is representative also for the cirrus above the lidar site.

The value of calculated RHi, together with the high value of cirrus mid-height temperature for this class (≈ −37 °C), indicates heterogeneous ice formation (Hagg et al., 2003). In our case a local source, which triggers the cirrus formation, could be ascribed to the aircraft exhaust. The lower value of LR_{eff} for class I could be associated to the formation of a large amount of small crystals due to the injection of WV by the aircraft engines.

For the other classes a reliable estimation of RHi has not been possible due to the weakness of the WV Raman signal at higher altitudes, which causes a relative uncertainty of more than 60 %, and the wet bias effect (approximately between 10–20 ppm) affecting the measurements above 10 km.

The same analysis of LR_{eff} in function of T_{mc} for thick cirrus is depicted in Fig. 6 (first and second rows for classes IIa and IIb, respectively). The two classes show different dependences. In particular, for class IIa, the LR_{eff} values slightly decrease with temperature lowering from −45 to −60 °C, while an opposite trend characterizes the class IIb from −30 to −50 °C. The different temperatures, at which the two classes are observed, could explain these behaviors. In fact, for the most part of the common temperature interval (between −50 and −60 °C), a similar decreasing trend is observed. A similar dependence was found by Whiteman et al. (2004) for hurricane-influenced observations and explained by a continuous supply of moisture from anvil outflows. Dedicated studies are needed to further investigate their attribution and origin. It is to be noted that, for the four classes, the dependence of LR_{eff} on optical depth and

ACPD
13, 9615–9652, 2013

effective height was also analyzed (not reported here), but no clear and significant tendencies were found.

To compare and evaluate the cirrus optical parameters in Table 4 with lidar measurements at similar latitudes, these parameters have been re-computed following the classification scheme of Sassen and Cho (1992). The obtained results are presented in Table 5. The observed relative occurrences for the three classes (10 %, 49 %, 41 %) are comparable to other mid-latitude measurements taken above central Europe (Reichardt et al., 1999, 10 %, 60 % and 30 %), over Greece (Giannakaki et al., 2007, 3 %, 57 % and 40 %), and Oklahoma (Wang and Sassen; 2002, 10 %, 65 % and 25 %) but differ from those above Utah (Sassen and Campbell, 2001, 10 %, 30 %, 60 %). A maximum occurrence for thin cirrus was also found by Goldfarb et al. (2001) above south France and by Immler and Schrems (2002) for northern and southern mid-latitude sites (Prestwick, Pr, and Punta Arenas, PA), while more SVC cirrus cases were measured (approximately 20 %). The estimated values of LR_{eff} (26, 29 and 32 sr for τ_{Rm} equal to 0.03, 0.17 and 0.69, respectively) for the three classes highlight an increasing trend of the lidar ratio with the rise of the cirrus optical depth. This tendency is in contradiction with the observations of the cirrus lidar ratio over Utah (Sassen and Comstock, 2001), where values of about 35, 27, 22, 22, and 21 sr were measured for optical depths around 0.12, 0.25, 0.5, 1, 1.2, and 2.5, respectively.

The overall mean value of τ_{Rm} (0.37 ± 0.18) is higher than to those derived by other midlatitude cirrus datasets, as Reichardt (1999, $\tau = 0.25$–0.30), Immler and Schrems (2002, $\tau = 0.28 \pm 0.11$ for Pr and $\tau = 0.27 \pm 0.08$ for PA), Lakkis et al. (2011, $\tau = 0.29 \pm 0.09$), and similar to Giannakaki et al. (2007, $\tau = 0.31$–0.34). Similarly the mean value of LR_{eff} (31 ± 15 sr) appears higher compared to mid-latitude measurements and agrees better with cirrus observed at lower latitudes, as above Taiwan (Chen, 2002, $LR = 29 \pm 12$ sr) or over the tropical Indian Ocean during northeast (NE) and southwest (SW) monsoon seasons ($LR = 33 \pm 9$ sr for NE and $LR = 29 \pm 11$ sr for SW).

ACPD
13, 9615–9652, 2013

4 Summary and conclusions

The dataset of RTV lidar, a multi-channel instrument (optimized for water vapor measurements), has been, for the first time, employed to characterize cirrus clouds. In particular, using the elastic and the Raman nitrogen channels of the system, the cirrus characteristics as effective height, geometrical and optical thickness and mean back-scattering ratio have been derived. The mid-height temperature inside the cloud, estimated through the radiosounde data of Pratica di Mare, 25 km southwest from RTV site, was added to integrate the dataset.

Defining the cirrus occurrence as the ratio of the number of cirrus detections on the total number of measurements, cirrus clouds were detected in 47 % of the operational days, a value similar to the one (45 %) measured by Gobbi et al. (2004) above the same site. However this percentage lowers to 30 % if the ratio of cirrus detection time on the total measurement time is taken into account. It is noteworthy that these statistics are derived for nighttime measurements acquired in absence of precipitation and of lower tropospheric clouds.

The characterization of the detected cirrus has been performed through a clustering multivariate analysis approach, previously adopted for the OHP lidar. This statistical method, applied to the RTV cirrus dataset for the period February 2007–April 2010 (93 lidar sessions, approximately 500 h of lidar acquisitions), allowed identifying four cirrus classes above the Italian site for the considered period: two thin cirrus clusters in mid and upper troposphere (class I and III, respectively) and two thick cirrus clusters in upper troposphere (class IIa and IIb).

The comparison of these results to the ones obtained by OHP analysis attests the validity both of the employment of RTV lidar on cirrus investigation and of the clustering method used. Thin cirrus classes, observed above the two sites, result to be very similar in terms of lidar parameters (cirrus effective height, geometrical and optical depth), while the thick cirrus class, identified at the OHP, seems to be split in two sub-classes in the RTV classification (classes IIa and IIb). The absolute cirrus occurrence is smaller on the Italian than on the French site (30 % vs. 37 %, respectively) while the occurrence of each cirrus class varies between the lidar stations, highlighting the fact that different weather patterns characterize the two sites.

With the objective of explaining the main physical processes that control these classes, the analysis of the effective lidar ratio of a subsample of cirrus cases (approximately 65 %) with $\Delta\tau_{Rm}/\tau_{Rm} \leq 30\,\%$ have been performed. Taking into account the associated errors, the frequency distribution functions of LR_{eff} values and their dependence to the mid-height cirrus temperature have been studied.

The calculated frequency distribution functions highlighted the optical similarities between classes IIa and IIb, where the functions are centered between 20 and 40 sr, and between classes I and III, characterized by an higher probability of LR_{eff} between 0 and 20 sr. Following the work of Reichardt et al. (2002), these results might attest that thin cirrus classes are composed by crystals smaller and more regular in shape compared to thick classes.

The increasing trend of LR_{eff} (from 10 to 45 sr) with temperature decreasing (from −25 to −40 °C), together with the value of RHi (110 ± 30 %), retrieved with the simultaneous WV Raman measurements, gave some indication that ice crystals could be formed by heterogeneous nucleation and a local source, such as aircraft exhausts, could be a possible origin of mid-tropospheric thin cirrus (class I).

It has to be noted that, in contrast to the latter hypothesis, the formation of higher tropopause thin cirrus (class III) is explained through the large-scale transport processes of moist tropical upper tropospheric air masses (Kekchut et al., 2005; Montoux et al., 2010).

The same analysis, conducted to thick cirrus (classes IIa and IIb), pointed out an opposite trends between the two clusters, probably connected to the different temperature ranges at which the two classes are observed (from −45 to −60 °C and from −30 to −60 °C, respectively). At the latitudes of the TVR site, these cirrus could be associated to mid-latitude cirrus preceding weather disturbances as indicated by the work

Discussion Paper | Discussion Paper | Discussion Paper | Discussion Paper |

ACPD

13, 9615–9652, 2013

Mid-latitude cirrus classification at Rome Tor Vergata

D. Dionisi et al.

of Sassen and Comstock (2003), but no significant indications on this way have been found.

The comparison of the RTV cirrus results with other lidar cirrus dataset through the classification scheme of Sassen and Cho (1992) are in good agreement with other mid-latitude lidar measurements regarding optical depth. In particular, these results confirm previous analyses of cirrus clouds with lidar that show that thin cirrus at mid-latitudes are present in a greater percentage (49 %) than thick or opaque cirrus (41 %).

For the LR_{eff}, most retrieved values ranged from 10–60 sr, in agreement with other works performed at different latitudes (Sassen and Comstock, 2001; Chen et al., 2002; Whiteman et al., 2004; Seifert et al., 2007) but in contrast with the values estimated by Platt et al. (2002) through LIRAD technique. The estimated mean value of LR_{eff} (31 ± 15 sr) agrees better with LR values of cirrus observed at lower latitudes than those calculated at similar latitudes. The reason for these similarities between cirrus at different latitudes is not known. Furthermore, a large uncertainty exists in the comparison of LR calculated by different systems due to possible different definitions of a single cirrus cloud layer as well as the approach to correct for multiple scattering effects and system setups.

Finally, the comparison between the clustering and the standard cirrus classification (Tables 4 and 5 in Sect. 3.2) shows that SVC cirrus clouds include classes I and III, thin cirrus are mainly formed by classes III and IIa and opaque cirrus correspond to class IIb and IIa. It is interesting to note that the classical cirrus subdivision does not allow distinguishing between the different heights (and origin) of the different classes, which, as in the case of classes I and III, can cause significant differences in terms of radiative impact. This confirms the fact that a cirrus classification using only optical depth as a discriminating factor is meaningful for practical purposes, but it does not provide any indication of the cirrus generating process.

On the contrary, the consistency of the obtained results suggests that a cirrus classification based on a statistical approach gives more indications on the physical mechanisms that govern these classes, and, consequently, could improve the estimation of

ACPD
13, 9615–9652, 2013

the associated LR values, which are important also for the validation and development of the algorithm adopted to calculate cirrus optical depth from space borne lidar as the Cloud-Aerosol Lidar with Orthogonal Polarization (CALIOP).

For these reasons, further studies with dedicated campaigns are planned to extend this procedure to other locations and to improve the characterisation of the optical properties of each class. With this aim, the RMR lidar configuration will be implemented to improve the WV measurement accuracy in the upper troposphere, reducing the statistical error and correcting the wet bias. This will permit to use the spatial and temporal information provided by the simultaneous lidar measurements of cirrus clouds and water vapour to investigate the key processes controlling cirrus formation and evolution and to ameliorate the knowledge of the water vapour vertical distribution in the upper troposphere.

Acknowledgements. The research leading to these results has received funding from the European Union Seventh Framework Programme (FP7/2007–2013) and University of Versailles and Saint Quentin en Yvelines (UVSQ) under grant agreement RBUCE-UP N° 246556. Radiosonde data are routinely supplied by the Italian Meteorological Service of the Military Aeronautics.

The publication of this article is financed by CNRS-INSU.

References

Ansmann, A., Wandinger, U., Riebesell, M., Weitkamp, C., and Michaelis, W.: Independent measurement of extinction and backscatter profiles in cirrus clouds by using a combined Raman elastic-backscatter lidar, Appl. Optics, 31, 7113–7113, 1992.

Borchi, F. and Marenco, A.: Discrimination of air masses near the extratropical tropopause by multivariate analyses from MOZAIC data, Atmos. Environ., 36, 1123–1135, 2002.

Brooks, I. M.: Finding boundary layer top: application of a wavelet covariance transform to lidar backscatter profiles, J. Atmos. Ocean. Tech., 20, 1092–1105, 2003.

Cadet, B., Giraud, V., Haeffelin, M., Keckhut, P., Rechou, A., and Baldy, S.: Improved retrievals of the optical properties of cirrus clouds by a combination of lidar methods, Appl. Opt., 44, 1726–1734, 2005.

Chen, W. N., Chiang, C. W., and Nee, J. W.: Lidar ratio and depolarization ratio for cirrus clouds, Appl. Optics, 41, 6470–6476, 2002.

Chepfer, H., Bony, S. D., Winker, M., Chiriaco, M., Dufresne, J. L., and Seze, G.: Use of CALIPSO lidar observations to evaluate the cloudiness simulated by a climate model, Geophys. Res. Lett., 35, L15704, doi:10.1029/2008GL034207, 2008.

Comstock, J. M., Ackerman, T. P., Mace, G. G.: Ground-based lidar and radar remote sensing of tropical cirrus clouds at Nauru Island: cloud statistics and radiative impacts, J. Geophys. Res., 107, 4714, doi:10.1029/2002JD002203, 2002.

Congeduti, F., Marenco, F., Baldetti, P., and Vincenti, E.: The multiple-mirror lidar “9-eyes”, J. Opt. A-Pure Appl. Op., 1, 185–191, 1999.

Davis, S., Hlavka, D., Jensen, E., Rosenlof, K., Yang, Q., Schmidt, S., Borrmann, S., Frey, W., Lawson, P., Voemel, H., and Bui, T. P.: In situ and lidar observations of tropopause subvisible cirrus clouds during TC4, J. Geophys. Res., 115, D00J17, doi:10.1029/2009JD013093, 2010.

Dinh, T. P., Durran, D. R., and Ackerman, T.: The maintenance of tropical tropopause layer cirrus, J. Geophys. Res., 115, D02104, doi:10.1029/2009JD012735, 2010.

Dionisi, D., Congeduti, F., Liberti, G. L., Cardillo, F.: Calibration of a multichannel water Vapor Raman Lidar through noncollocated operational soundings: optimization and characterization of accuracy and variability, J. Atmos. Ocean. Tech., 27, 108–121, 2010.

Dupont, J. C., Haeffelin, M., Morille, Y., Noël, V., Keckhut, P., Winker, D., Comstock, J., Chervet, P., and Roblin, A.: Macrophysical and optical properties of midlatitude cirrus clouds from four ground-based lidars and collocated CALIOP observations, J. Geophys. Res., 115, D00H24, doi:10.1029/2009JD011943, 2010.

Giannakaki, E., Balis, D. S., Amiridis, V., and Kazadzis, S.: Optical and geometrical characteristics of cirrus clouds over a Southern European lidar station, Atmos. Chem. Phys., 7, 5519–5530, doi:10.5194/acp-7-5519-2007, 2007.

ACPD
13, 9615–9652, 2013

Mid-latitude cirrus classification at Rome Tor Vergata

D. Dionisi et al.

Gobbi, G. P., Barnaba, F., and Ammannato, L.: The vertical distribution of aerosols, Saharan dust and cirrus clouds in Rome (Italy) in the year 2001, Atmos. Chem. Phys., 4, 351–359, doi:10.5194/acp-4-351-2004, 2004.
Goldfarb, L., Keckhut, P., Chanin, M. L., and Hauchecorne, A.: Cirrus climatological results from lidar measurements at OHP, Geophys. Res. Lett., 28, 1687–1690, 2001.
Haag, W., Kärcher, B., Ström, J., Minikin, A., Lohmann, U., Ovarlez, J., and Stohl, A.: Freezing thresholds and cirrus cloud formation mechanisms inferred from in situ measurements of relative humidity, Atmos. Chem. Phys., 3, 1791–1806, doi:10.5194/acp-3-1791-2003, 2003.
Haij, M. J. D., Klein Baltink, H.: Continuous mixing layer height determination using the LD-40 ceilometer: a feasibility study KNM I, Scientific Report WR, Koninklijk Nederlands Meteorologisch Instituut, Holland, 2007.
Haladay, T. and Stephens, G.: Characteristics of tropical thin cirrus clouds deduced from joint CloudSat and CALIPSO observations, J. Geophys. Res., 114, D00A25, doi:10.1029/2008JD010675, 2009.
Hoareau, C., Keckhut, P., Sarkissian, A., Baray, J. L., and Durry, G.: Methodology for water monitoring in the upper troposphere with Raman lidar at Haute-Provence Observatory, J. Atmos. Ocean. Tech., 26, 2149–2160, 2009.
Hoareau, C., Keckhut, P., Baray, J.-L., Robert, L., Courcoux, Y., Porteneuve, J., Vömel, H., and Morel, B.: A Raman lidar at La Reunion (20.8° S, 55.5° E) for monitoring water vapour and cirrus distributions in the subtropical upper troposphere: preliminary analyses and description of a future system, Atmos. Meas. Tech., 5, 1333–1348, doi:10.5194/amt-5-1333-2012, 2012.
Hoareau, C., Keckhut, P., Noel, V., Chepfer, H., and Baray, J.-L.: A decadal cirrus clouds climatology from ground-based and spaceborne lidars above south of France (43.9° N–5.7° E), Atmos. Chem. Phys. Discuss., 13, 6379–6417, doi:10.5194/acpd-13-6379-2013, 2013.
Immler, F. and Schrems, O.: Lidar measurements of cirrus clouds in the northern and southern midlatitudes during INCA (55° N, 53° S): a comparative study, Geophys. Res. Lett., 29, 1809, doi:10.1029/2002GL015077, 2002.
Immler, F., Treffeisen, R., Engelbart, D., Krüger, K., and Schrems, O.: Cirrus, contrails, and ice supersaturated regions in high pressure systems at northern mid latitudes, Atmos. Chem. Phys., 8, 1689–1699, doi:10.5194/acp-8-1689-2008, 2008.
Jolliffe, I. T.: Principal Component Analysis, Springer, 502 pp., New York, 1986.

Keckhut, P., Hauchecorne, A., Bekki, S., Colette, A., David, C., and Jumelet, J.: Indications of thin cirrus clouds in the stratosphere at mid-latitudes, Atmos. Chem. Phys., 5, 3407–3414, doi:10.5194/acp-5-3407-2005, 2005.

Keckhut, P., Borchi, F., Bekki, S., Hauchecorne, A., and SiLaouina, M.: Cirrus classification at mid-latitude from systematic lidar observations, J. Appl. Meteorol. Clim., 45, 249–258, 2006.

Khvorostyanov, V. I. and Sassen, K.: Microphysical processes in cirrus and their impact on radiation: a mesoscale modeling perspective, in: Cirrus, edited by: Lynch, D. K., Sassen, K., Starr, D. O' C., and Stephens, G., Oxford University Press, 397–432, 2002.

Lanzante, J. R.: Resistant, Robust and non-parametric techniques for the analysis of climate data: theory and examples, including applications to historical radiosonde station data, Int. J. Climatol., 16, 1197–1226, 1996.

Lohmann, U., Karcher, B., and Hendricks, J.: Sensitivity studies of cirrus clouds formed by heterogeneous freezing in the ECHAM GCM, J. Geophys. Res., 109, D16204, doi:10.1029/2003JD004443, 2004.

Montoux, N., Keckhut, P., Hauchecorne, A., Jumelet, J., Brogniez, H., and David, C.: Isentropic modeling of a cirrus cloud event observed in the midlatitude upper troposphere and lower stratosphere, J. Geophys. Res., 115, D02202, doi:10.1029/2009JD011981, 2010.

Lakkis, S., Lavorato, M., Canziani, P., and Lacomi, H.: Cirrus clouds and multiple tropopause events over Buenos Aires, Atmospheric and Climate Sciences, 1, 113–119, doi:10.4236/acs.2011.13013, 2011.

Luo, Z. and Rossow, W. B.: Characterizing tropical cirrus life cycle, evolution, and interaction with upper-tropospheric water vapor using lagrangian trajectory analysis of satellite observations, J. Climate, 17, 4541–4563, 2004.

Platt, C. M. R. and Dilley, A. C.: Determination of the cirrus particle single-scattering phase function from lidar and solar radiometric data, Appl. Optics, 23, 380–386, 1984.

Reichardt, J.: Optical and geometrical properties of northern mid-latitude cirrus clouds observed with a UV Raman lidar, Phys. Chem. Earth Pt. B, 24, 255–260, 1999.

Reichardt, J., Reichardt, S., Hess, M., and McGee, T. J.: Correlations among the optical properties of cirrus-cloud particles: Microphysical interpretation, J. Geophys. Res., 107, 4562, doi:10.1029/2002JD002589, 2002.

Riihimaki, L. D. and McFarlane, S. A.: Frequency and morphology of tropical tropopause layer cirrus from CALIPSO observations: are isolated cirrus different from those connected to deep convection?, J. Geophys. Res., 115, D18201, doi:10.1029/2009JD013133, 2010.

ACPD
13, 9615–9652, 2013

Sanderson, B. M., Piani, C., and Ingram, W. J.: Towards constraining climate sensitivity by linear analysis of feedback patterns in thousands of perturbed-physics GCM simulations, Clim. Dynam., 30, 175–190, doi:10.1007/s00382-007-0280-7, 2008.

Sassen, K. and Campbell, J. R.: A midlatitude cirrus cloud climatology from the Facility for Atmospheric Remote Sensing, Part I: Macrophysical and synoptic properties, J. Atmos. Sci., 58, 481–496, 2001.

Sassen, K. and Cho, B. Y.: Subvisual-thin cirrus lidar dataset for satellite verification and climatological research, J. Appl. Meteorol., 31, 1275–1285, 1992.

Sassen, K. and Comstock, J. M.: A midlatitude cirrus cloud climatology from the Facility for Atmospheric Remote Sensing, Part III: Radiative properties, J. Atmos. Sci., 58, 2113–2127, 2001.

Sassen, K., Wang, Z., and Liu, D.: Cirrus clouds and deep convection in the tropics: insights from CALIPSO and CloudSat, J. Geophys. Res., 114, D00H06, doi:10.1029/2009JD011916, 2009.

Seifert, P., Ansmann, A., Müller, D., Wandinger, U., Althausen, D., Heymsfield, A. J., Massie, S. T., and Schmitt, C.: Cirrus optical properties observed with lidar, radiosonde, and satellite over the tropical Indian Ocean during the aerosol-polluted northeast and clean maritime southwest monsoon, J. Geophys. Res., 112, D17205, doi:10.1029/2006JD008352, 2007.

Solomon, S., Qin, D., Manning, M., Alley, R. B., Berntsen, T., Bindoff, N. L., Chen, Z., Chidthaisong, A., Gregory, J. M., Hegerl, G. C., Heimann, M., Hewitson, B., Hoskins, B. J., Joos, F., Jouzel, J., Kattsov, V., Lohmann, U., Matsuno, T., Molina, M., Nicholls, N., Overpeck, J., Raga, G., Ramaswamy, V., Ren, J., Rusticucci, M., Somerville, R., Stocker, T. F., Whetton, P., Wood, R. A., and Wratt, D.: Technical summary, in: Climate Change 2007: The Physical Science Basis, Contribution of Working Group I to the Fourth Assessment Report of the Intergovernmental Panel on Climate Change, edited by: Solomon, S., Qin, D., Manning, M., Chen, Z., Marquis, M., Averyt, K. B., Tignor, M., and Miller, H. L., Cambridge University Press, Cambridge, UK, New York, NY, USA, 2007.

Ström, J., Seifert, M., Kärcher, B., Ovarlez, J., Minikin, A., Gayet, J.-F., Krejci, R., Petzold, A., Auriol, F., Haag, W., Busen, R., Schumann, U., and Hansson, H. C.: Cirrus cloud occurrence as function of ambient relative humidity: a comparison of observations obtained during the INCA experiment, Atmos. Chem. Phys., 3, 1807–1816, doi:10.5194/acp-3-1807-2003, 2003.

ACPD
13, 9615–9652, 2013

Mid-latitude cirrus classification at Rome Tor Vergata

D. Dionisi et al.

Stubenrauch, C., Rossow, W., Scott, N., and Chedin, A.: Clouds as seen by satellite sounders (3I) and imagers (ISCCP), Part III: Spatial heterogeneity and radiative effects, J. Climate, 12, 3419–3442, 1999.

Van de Hulst, J. C.: Light Scattering by Small Particles, Dover, New York, 1957.

Wandinger, U.: Multiple-scattering influence on extinction- and backscatter-coefficient measurements with Raman and high-spectral resolution lidars, Appl. Optics, 37, 417–427, 1998.

Wang, Z. and Sassen, K.: Cirrus cloud microphysical property retrieval using lidar and radar measurements: II. Midlatitude cirrus microphysical and radiative properties, J. Atmos. Sci., 59, 2291–2302, 2002.

Ward, J. H.: Hierarchical grouping to optimize an objective function, J. Am. Stat. Assoc., 58, 236–244, 1963.

Whiteman, D. N., Demoz, B., Wang, Z.: Subtropical cirrus cloud extinction to backscatter ratios measured by Raman Lidar during CAMEX-3, Geophys. Res. Lett., 31, L12105, doi:10.1029/2004GL020003, 2004.

WMO: Meteorology – a three-dimensional science, WMO Bull., 6, 134–138, 1957.

Zhang, M. H., Lin, W. Y., Klein, S. A., Bacmeister, J. T., Bony, S., Cederwall, R. T., Del Genio, A. D., Hack, J. J., Loeb, N. G., Lohmann, U., Minnis, P., Musat, I., Pincus, R., Stier, P., Suarez, M. J., Webb, M. J., Wu, J. B., Xie, S. C., Yao, M. S., and Zhang, J. H.: Comparing clouds and their seasonal variations in 10 atmospheric general circulation models with satellite measurements, J. Geophys. Res., 110, D15S02, doi:10.1029/2004JD005021, 2005.

ACPD

13, 9615–9652, 2013

Mid-latitude cirrus classification at Rome Tor Vergata

D. Dionisi et al.

Table 1. Transmitter and receiver characteristics of the RTV lidar system.

	RTV (41.8° N, 12.6° E, 107 m a.s.l.)		
Transmitter			
Laser Type	Nd:Yag		
Wavelenght	532–355 nm		
Energy per pulse	200–400 mJ		
Pulse repetition rate	10 Hz		
beam diameter	45 mm		
beam divergence	0.1 mrad		
Receiver	Collector 1	Collector 2	Collector 3
Type of telescope	Newtonian array	Newtonian	Newtonian
Diameter, f number	9 × 500 mm, F3	300 mm, F3	150 mm, F3
Field of view (mrad)	0.6	0.9	1.8
Optic fiber	yes	yes	yes
Data acquisition			
Raman channels N_2	387 nm	387 nm	
H_2O	407 nm	407 nm	
Elastic channels	532 nm	532 nm	532 nm
Sounding range (km)	2–15 (Raman)	0.1–5 (Raman)	
	25–80 (elastic)	6–40 (elastic)	0.5–14 (elastic)
Time resolution (s)	60	60	60
Vertical resolution (m)	75	75	75

ACPD
13, 9615–9652, 2013

Mid-latitude cirrus classification at Rome Tor Vergata

D. Dionisi et al.

Table 2. Characteristics of cirrus dataset for the period 2007–2010.

	# Lidar sessions	Daily and absolute cirrus occurrence	# Cirrus	# Cirrus multilayer
RMR dataset (2007–2010)	93	47–30 %	167	29

ACPD
13, 9615–9652, 2013

Table 3. Principal lidar parameters of the cirrus classes identified by multivariate analysis applied at the RTV dataset (2007–2010). Temperature values are derived from the operational radiosoundings launched from Pratica di Mare (25 km south-west from RTV). In the last part of the table, the lidar parameters of the cirrus classes identified at OHP by the same analysis are listed.

RTV	I: Midtropo. thin cirrus	IIa: Upper tropo. cirrus	IIb: Upper tropo. cirrus	III: Thin tropopause cirrus	IV: Episodic highly scattering cirrus
Rel. occurrence [%]	17	30	21	30	2
Abs. Occurence [%]	5	9	6	9	< 1
Geometric height [km]	7.8 ± 0.9	10.2 ± 0.9	8.8 ± 0.9	11.2 ± 0.7	10.9 ± 1.6
Thickness [km]	1.2 ± 0.7	2.8 ± 0.6	4.3 ± 0.8	1.3 ± 0.5	3.1 ± 0.5
Intensity of the mean SR	3.4 ± 2.3	10.0 ± 6.4	15.4 ± 8.1	6.3 ± 6.3	64.9 ± 14.8
Mid cloud temperature [°C]	-36 ± 7	-53 ± 4	-42 ± 7	-58 ± 4	-53 ± 11
Optical depth (a-priori LR)	0.04 ± 0.06	0.16 ± 0.20	0.47 ± 0.36	0.09 ± 0.09	1.62 ± 1.09
OHP	I: Midtropo. thin cirrus	II: Upper tropo. cirrus		III: Thin tropopause cirrus	IV: Episodic highly scattering cirrus
Abs. occurrence [%]	10	11		15	< 1
Geometric height [km]	8.6 ± 0.9	9.8 ± 0.7		11.5 ± 0.9	10.6 ± 0.3
Thickness [km]	0.9 ± 0.6	3.2 ± 0.9		0.9 ± 0.6	1.0 ± 0.8

ACPD
13, 9615–9652, 2013
Mid-latitude cirrus classification at Rome Tor Vergata
D. Dionisi et al.

Table 4. Mean optical parameters for each cirrus class derived for a subsample of cirrus cases with $\Delta\tau_{\mathrm{Rm}}/\tau_{\mathrm{Rm}} \leq 30\,\%$. The fractions of the total lidar observations used for these results are given in parentheses.

Class type	I: Midtropo. thin cirrus	IIa: Upper tropo. cirrus	IIb: Upper tropo. cirrus	III: Thin tropopause cirrus
# Cirrus	18 (60 %)	34 (70 %)	30 (82 %)	25 (47 %)
Optical depth (a-priori LR)	0.08 ± 0.07	0.21 ± 0.19	0.46 ± 0.31	0.15 ± 0.07
Optical depth (Raman)	0.10 ± 0.08	0.31 ± 0.31	0.75 ± 0.47	0.21 ± 0.10
Effective LR [sr]	28 ± 14	31 ± 10	32 ± 9	29 ± 18
SR mass center relative position	0.50 ± 0.07	0.52 ± 0.08	0.51 ± 0.09	0.56 ± 0.06

ACPD
13, 9615–9652, 2013

Table 5. Frequency, mean optical depth (Raman method), effective Lidar Ratio and backscattering mass center relative position for the subsample of cirrus dataset divided following Sassen and Cho (1992) classification scheme.

Class type	Subvisible Cirrus, $\tau < 0.03$	Thin Cirrus, $0.03 < \tau < 0.3$	Opaque Cirrus, $\tau > 0.3$	All Cirrus
Frequency [%]	10	49	41	–
Optical depth (Raman)	0.026 ± 0.007	0.17 ± 0.09	0.69 ± 0.32	0.37 ± 0.18
Effective LR [sr]	26 ± 20	29 ± 15	32 ± 11	31 ± 22
SR mass center relative position	0.54 ± 0.05	0.53 ± 0.08	0.52 ± 0.10	0.52 ± 0.10

ACPD
13, 9615–9652, 2013

Mid-latitude cirrus classification at Rome Tor Vergata

D. Dionisi et al.

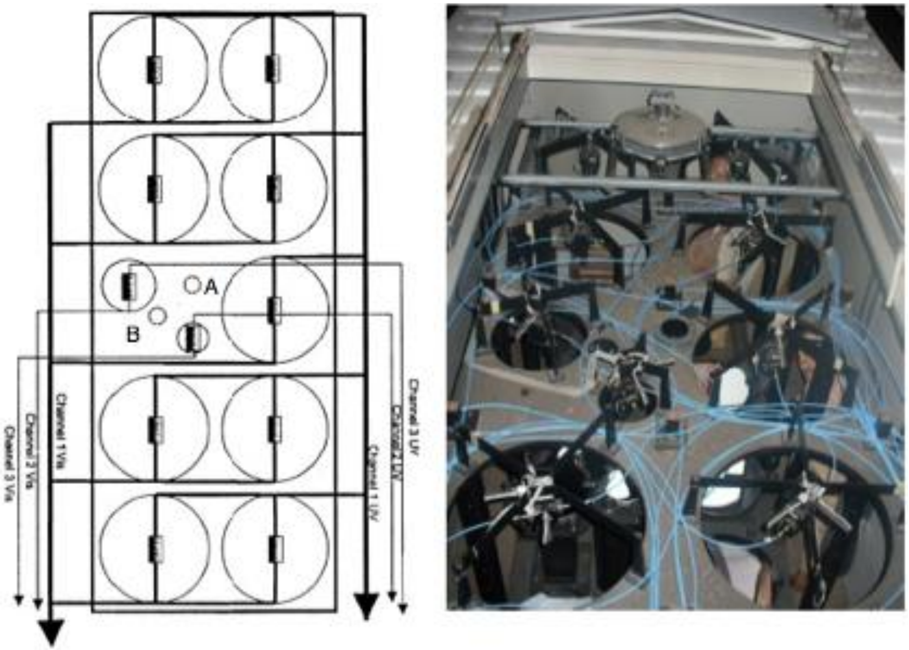

Fig. 1. Diagram of the RMR receiving channels (left) with their corresponding bird'eye view (right). A and B on the diagram are the exit holes for the upward laser beam at 532 and 355 nm, respectively.

ACPD
13, 9615–9652, 2013

Mid-latitude cirrus classification at Rome Tor Vergata

D. Dionisi et al.

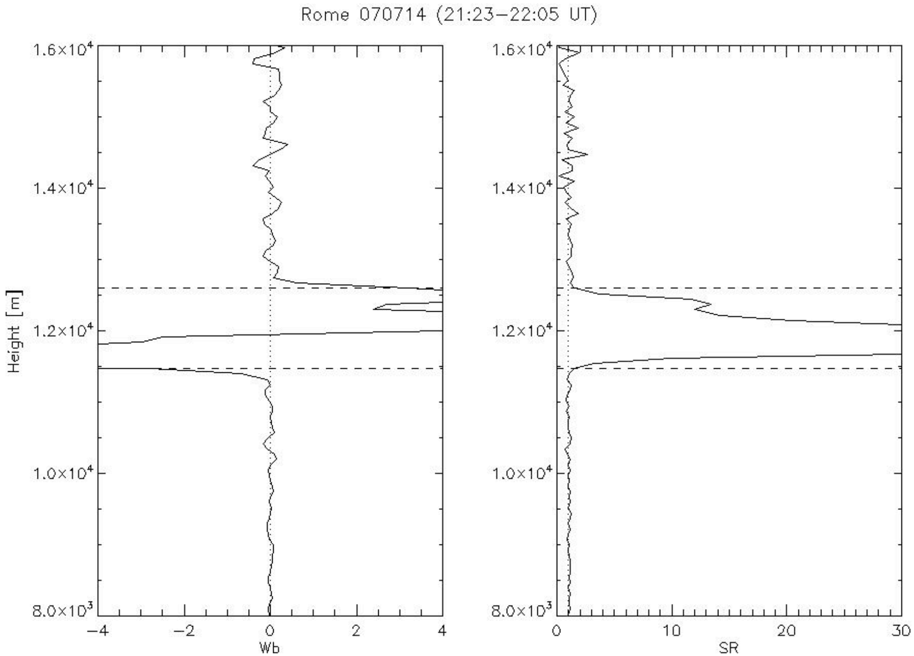

Fig. 2. SR(z) profile (right panel) for a cirrus observed during the night of 5 July 2012, between 21:23 and 22:05 UT with the corresponding $W_b(z)$ profile. The dashed horizontal lines on the left panel mark the inflection points of W_b to which correspond the bottom (11 469 m) and the top (12 519 m) of the cirrus on the right panel.

ACPD
13, 9615–9652, 2013

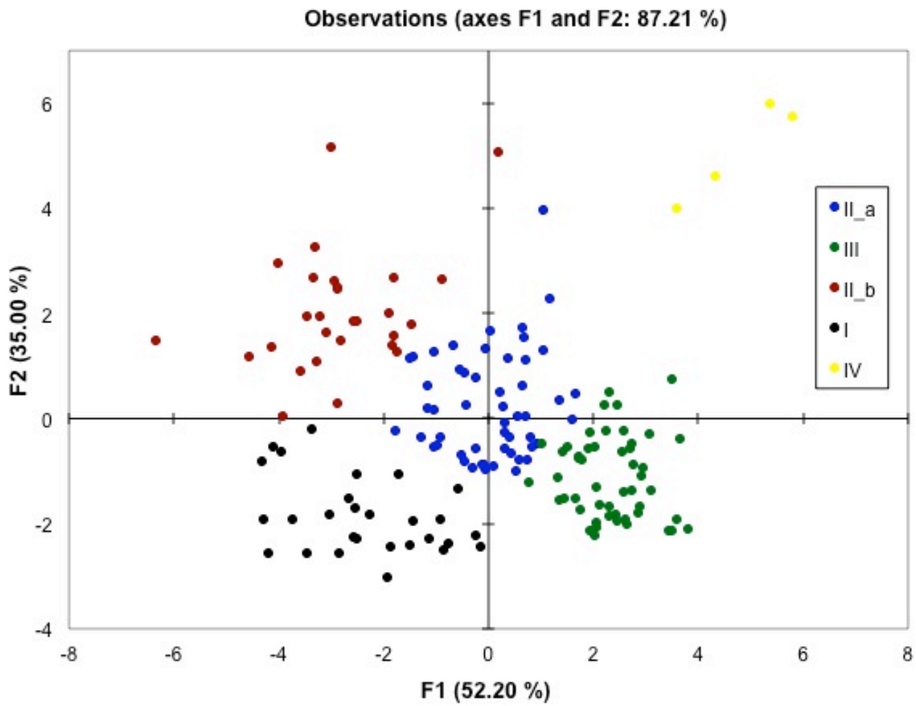

Fig. 3. Cirrus parameters represented (projected) on the two sets of orthogonal axes identified by the DFA, which describe the 87.21 % of the cirrus characteristics. Colored dots identify the different classes discriminated by HCM.

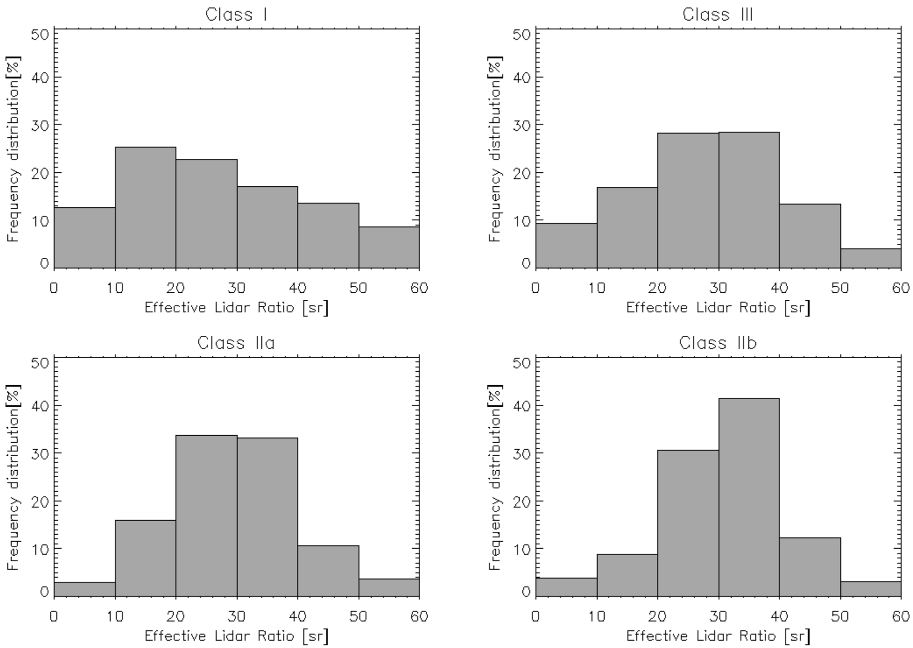

Fig. 4. Frequency distribution functions of LR_{eff} computed for the four cirrus classes. Each LR_{eff} value has been assumed to have a Gaussian shape, which is determined by LR_{eff} and the associated error ΔLR_{eff}.

ACPD
13, 9615–9652, 2013

Mid-latitude cirrus classification at Rome Tor Vergata

D. Dionisi et al.

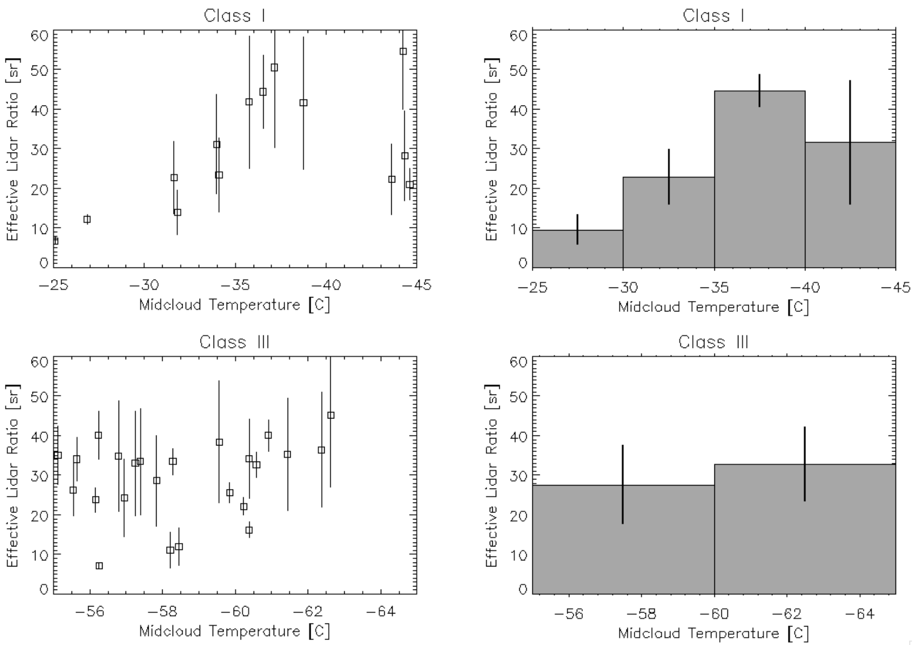

Fig. 5. Effective LR in function of midcloud temperature for classes I and III (first and second rows, respectively). In the first column single LR values together with their uncertainties (black vertical lines) are plotted in funtions of midcloud temperatureare, while the second column represents the frequency distributions of LR-weighted means with respect to midcloud temperature intervals of 5 K. The black vertical lines are the uncertainties of the single values and the standard deviations of the weighted means (first and second columns, respectively).

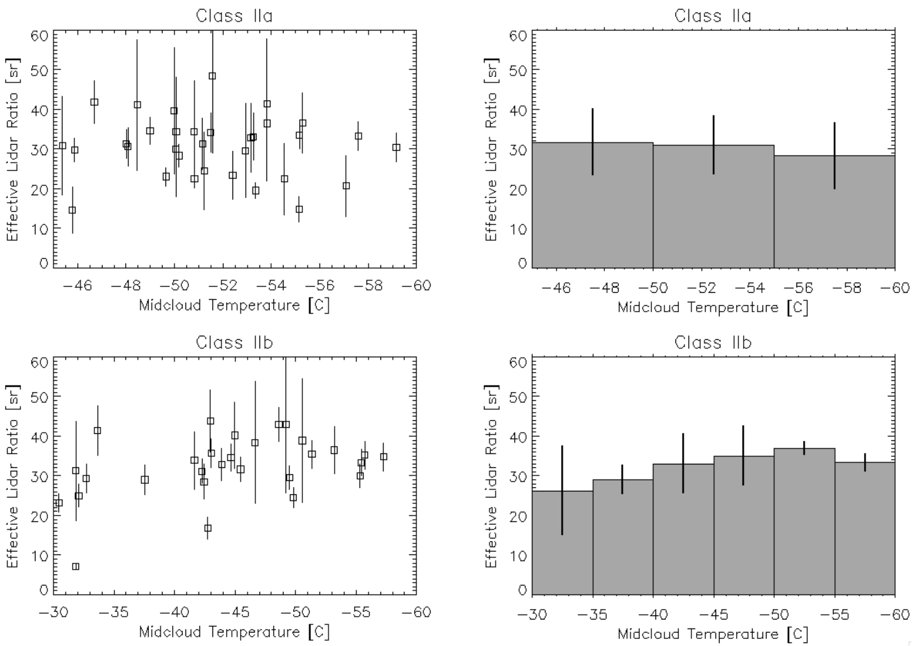

Fig. 6. Effective LR in function of midcloud temperature for classes IIa and IIb (first and second rows, respectively). In the first column single LR values together with their uncertainties (black vertical lines) are plotted in funtions of midcloud temperatureare, while the second column represents the frequency distributions of LR-weighted means with respect to midcloud temperature intervals of 5 K. The black vertical lines are the uncertainties of the single values and the standard deviations of the weighted means (first and second columns, respectively).

ACPD
13, 9615–9652, 2013

Mid-latitude cirrus classification at Rome Tor Vergata

D. Dionisi et al.